IOP Conf. Series: Materials Science and Engineering **425** (2018) 012026 doi:10.1088/1757-899X/425/1/012026

Analytical and numerical prediction of the flow and performance in a claw vacuum pump

J Willie

Chief Engineer, Innovation and Technology, Industrials Group, Gardner Denver Schopfheim GmbH, Johann-Sutter-Straße 6+8, 79650 Schopfheim, Germany

E-mail: James.Willie@gardnerdenver.com

Abstract. This paper presents the use of a 0-D thermodynamic chamber model and 3D Computational Fluid Dynamics (CFD) to predict the performance of a claw vacuum pump. The 0-D model can be used for pump sizing during the initial design or concept phase. Parameters such as the compression ratio (π), the built-in volume ratio (θ), the volumetric efficiency (η_V), the isentropic efficiency (η_{is}), the volume compression ratio (v_i) and the intermediate pressures (p_z, p_i) are essential to the performance of such machines. To determine these parameters, the volume-curve of the pump is determined as a function of the rotational angle. Using this model, it is possible to enhance the pump performance. For example, by decreasing the carry-over volume and by limiting or preventing over and under compression which can lead to an increase in the power consumption. This paper presents the results of the 0-D thermodynamic chamber model followed by the results of the 3D CFD simulations and validation with measurement data. After the benchmarking, CFD was used to improve the aerodynamic design of the pump discharge tube which led to a decrease in the power consumption of the pump compared to the baseline case. The diffuser angle was decrease to limit the boundary layer size and flow separation and recirculation at the discharge. When left unchecked, it can lead to large pressure drop and to an increase in the power consumption. Using CFD, other phenomenon such as such as pressure jump, which is commonplace in such machines, can be prevented. Otherwise, it can lead to shock wave generation and to noise in the pump.

1. Introduction

Modeling and simulation are playing an increasing role in the development process at Gardner Denver (GD). This reduces development time by reducing expensive tests in the laboratory. The availability of computing power at a relatively lower cost also makes modeling larger cases using finer meshes possible in industry. This paper presents one such example of how a 0-D chamber model and Computational Fluid Dynamics (CFD) can be used to help in the development and optimization process of vacuum pumps. Specifically, a claw vacuum pump is presented in this work. Based on the current knowledge of the author very little is available in the literature about these types of pumps, although they are used extensively in the vacuum industry. They are commonplace in the vacuum industry but the ultimate vacuum they can reach is limited by the temperature of the gas and the thermal loads on the rotors and bearings and sealing. The flow inside these pumps are influenced by many factors, for example, the opening and closing of the discharge contour, rotors profile and form, profile and housing gaps, the carried-over volume or dead volume, over-and under compression, the sealing, and so on. The tiny gaps inside these machines means that rotor to rotor contact or rotor to housing contact is possible.

This may damage the rotors or increase the pump power consumption. In the beginning of the design process the pump needs to be sized and to do this the 0-D model presented can be used. After the concepts development, 3D CFD is used to model the flow inside the pump including 3D effects like turbulence, etc. Flow optimization to reduce the pressure drop and increase the pumping speed or reduce the pump power can be performed using CFD. In this work, for example, engineering optimization is performed by changing the discharge tube geometry with the aim of lowering the pump power. The final goal of this work, which is not reported here, is to do conjugate heat transfer (CHT) analysis in order to determine the thermal loads on the rotors. The determined thermal and pressure loads can be exported to a structural code like Ansys Mechanical [1] to do Fluid-Structure Interaction (FSI) simulation to determine the deformation of the rotors and hence the hot gaps inside the pump.

Some applications of claw vacuum pumps include the following: Chemical industry, Environmental engineering (Aeration, drying, dust extraction, etc.), Industrial applications, Medical industry, Packaging industry, Pneumatic conveying, Post-press applications, Printing press, Wood working industry, and so on.

In the following, the 0-D thermodynamic chamber model is presented. This is followed by a description of the CFD set up used. After this, the measurement setup is presented followed by the results and discussions. Finally, the conclusions and future work are presented.

2. Thermodynamic chamber model

The schematics of a claw pump and the chamber volumes used in the 0-D thermodynamic chamber models are shown in Figure 1. The claw pump consists of two rotors in the form of a claw that rotate in opposite direction with one rotor (referred to as the male) bigger than the smaller rotor referred to as the female rotor. Both rotors are driven at the same speed with the female rotor transporting a larger volume of the working fluid, usually air. The torque generated and hence the power it consumes is therefore larger than that generated by the male rotor.

The working principle is shown in six steps in Figure 1(b) and described as follows [2]. In steps 1 and 2, air is taken into the pump. In step 3, the two closed volumes are transported by the rotors in an isochoric process that is assumed to be isobaric in the 0-D model. This is, however, not the case in reality because some compression takes place during the transport phase as shown in Figure 2. This diagram shows the p-V plot obtained by monitoring the pressure trace inside the pump at a normalized suction pressure of 0.36 in the CFD simulation compared to that obtained using the 0-D model. The power consumption is equal to the area bounded by the respective curve and the p-axis. In the chamber model the isochoric transport phase is assumed to be isobaric and therefore corresponds to only one point, namely, the point of maximum volume in the diagram. In the CFD simulations a rise in pressure occurs during the transport phase because of the gap flow and the heating inside the machine due to internal compression. The isothermal assumption used in the 0-D model is therefore only for simplicity. The CFD results show that we have over-compression at this suction pressure, even though it corresponds to our design point. The actual internal compression starts in step 4 and the carried-over volume is transported to the suction side. In step 5, the outlet begins to open, indicating that the internal compression is completed. Finally, in step 6, the volume is released at atmospheric pressure. A silencer is usually connected at the discharge to limit the pulsation caused by the lobe passing frequencies of the pump and the flow induced noise inside the pump at higher frequencies.

Based on the description above the equations of the 0-D thermodynamic model can be derived as presented below [2]. In the presented model equations the gap flows are neglected as well as heat transfer. The intermediate pressure p_z is given as a function of the chamber volumes and the suction pressure (p_S) as shown in equation 1:

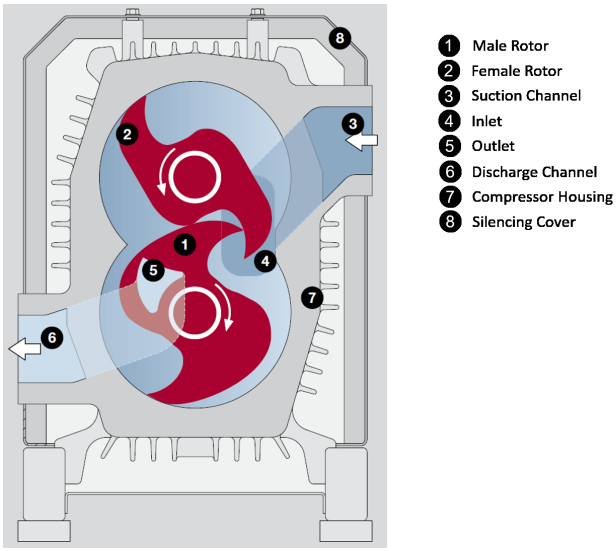

(a) Schematic of a claw pump

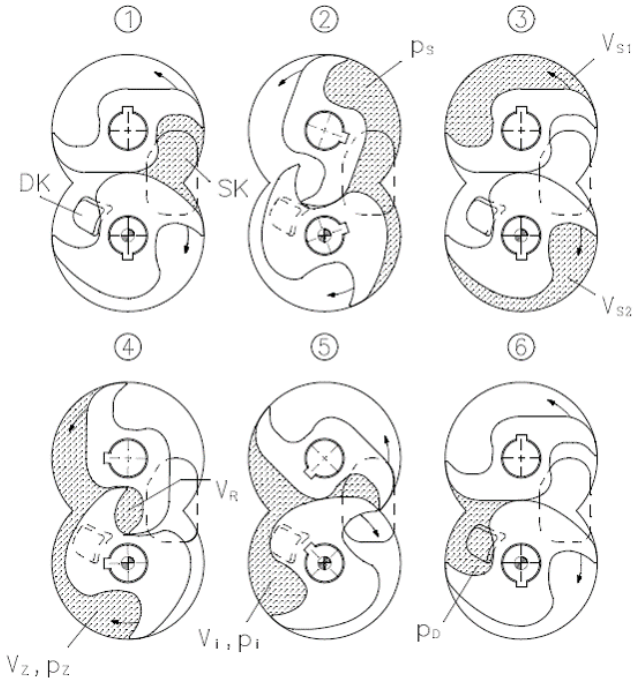

(b) Schematic of the chamber volumes used in model equations

Figure 1. Schematic of the claw vacuum pump and the chamber volumes used in the thermodynamic 0-D equations

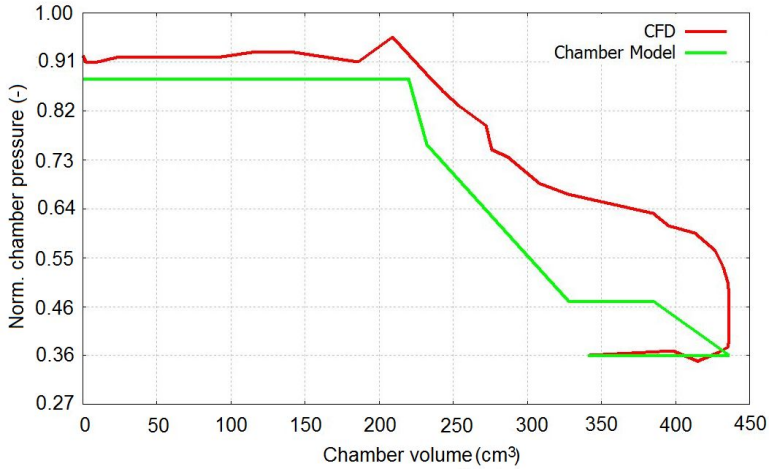

Figure 2. p-V Diagram of a typical claw pump operating at a normalized suction pressure of 0.36

$$p_z = p_S \left(\frac{V_{S1} + V_{S2}}{V_Z + V_R} \right) \tag{1}$$

The volume of the carried-over mass, V_{RS}, can be written as:

$$V_{RS} = V_R \left(\frac{p_z}{p_S} \right)^{\frac{1}{\kappa}}, \tag{2}$$

where V_R is the carried-over volume. Using this volume flow, the theoretical or ideal pumping speed of the pump can be expressed as:

$$\dot{V}_{th} = z(V_{S1} + V_{S2} - V_{RS})N, \tag{3}$$

where z is the number of rotor teeth and N is the rotational speed in Hz or 1/s. The maximum internal compression pressure just before the opening of the outlet is:

$$p_i = p_z \left(\frac{V_z}{V_i} \right)^{\kappa} = p_S \left(\frac{(V_{S1} + V_{S2})V_Z}{(V_Z + V_R)V_i} \right)^{\kappa} \tag{4}$$

The internal compression π is defined as:

$$\pi = \frac{p_i}{p_S} \tag{5}$$

Similarly, the internal volume ratio θ is given by:

$$\theta = \pi^{1/\kappa} = \left(\frac{(V_{S1} + V_{S2})V_Z}{(V_Z + V_R)V_i} \right) \tag{6}$$

The power taken by the pump is defined by the integral $\oint V dp$. Using the relationships above the power needed for isentropic compression (with no under or over-compression) and also not accounting for the partial compression of the carried-over volume is given by:

$$P_{is} = \frac{\kappa}{\kappa - 1} p_S \dot{V}_{th} \left[\left(\frac{P_D}{p_S} \right)^{\frac{(\kappa-1)}{\kappa}} - 1 \right] \tag{7}$$

If the pump is run at an off-design point (with under or over-compression), the theoretical isentropic power consumption becomes:

$$P^*_{is} = \frac{\kappa}{\kappa - 1} p_S \dot{V}_{th} \left(\left(\frac{P_i}{p_S} \right)^{\frac{(\kappa-1)}{\kappa}} - 1 \right) + (p_D - p_i)\dot{V}_i \tag{8}$$

Alternatively, equation 8 can be written as:

$$P^*_{is} = p_S \dot{V}_{th} \left[\frac{\kappa}{\kappa - 1} \left(\frac{1}{\kappa} \theta^{\kappa-1} - 1 \right) + \frac{p_D}{p_S} \frac{1}{\theta} \right] \tag{9}$$

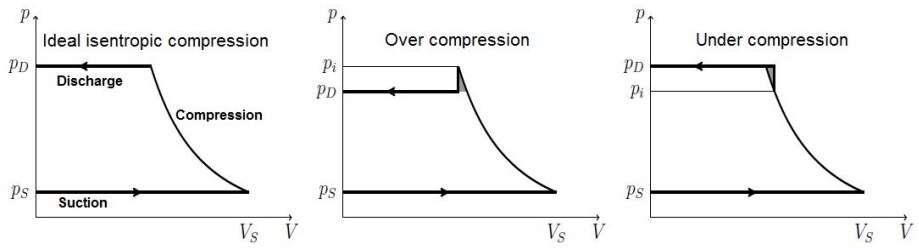

Figure 3. Schematic showing under and over-compression [3]

The power consumption calculated with equations 7 to 9 can be shown in the p-V diagram in Figure 3. Generally, three cases can be distinguished. The ideal case shown on the left where the pressure inside the pump housing at the discharge p_i is equal to the discharge pressure p_D when the discharge opens and the compression is isentropic. In the middle plot and just before the discharge opens the chamber pressure is greater than the discharge pressure and when the discharge opens the chamber pressure drops suddenly from p_i to p_D. The shaded area corresponds to the extra work that must be done because of the over-compression. In the sketch on the right the chamber pressure p_i is less than the discharge pressure before the discharge port is opened and it is referred to as under-compression. When the discharge opens a rapid flow is generated from the discharge tube to the chamber until we have an equalization of pressure. The extra work done as a result of the under-compression is shaded in the p-V diagram.

One possible deduction from equation 9 can be done by looking at the condition $\frac{\partial P^*_{is}}{\partial p_S} = \dot{V}_{th} \left[\frac{\kappa}{\kappa-1} \left(\frac{1}{\kappa} \theta^{\kappa-1} - 1 \right) \right] = 0$. This can be interpreted as the condition that must be satisfied in order for the power consumption of the pump to remain constant at all suction pressures.

Using the models above, performance parameters like the volumetric efficiency (η_V) and the isentropic efficiency (η_{is}) can be computed if the shaft power, $P_{shaft} = 2\pi TN$, where T is shaft torque, is known. The ideal volumetric efficiency (from the 0-D model) is given by:

$$\eta_{Vi} = \frac{\dot{V}_{th}}{\dot{V}_S}, \tag{10}$$

where $\dot{V}_S$ is the ideal volume flow rate given by:

$$\dot{V}_S = z(V_{S1} + V_{S2})N \tag{11}$$

Analogously, the real volumetric efficiency (η_{Vr}) is computed using the measured volume flow rate and given by:

$$\eta_{Vr} = \frac{\dot{V}_{measured}}{\dot{V}_S}, \tag{12}$$

The ideal volumetric flow rate does not depend on the suction pressure and therefore is constant where as the real volumetric flow rate depends on the suction pressures and decreases as the gap flow increases at lower suction pressures. For the volumetric efficiency computed from CFD, the numerator in equation 10 or 12 is replaced by the volume flow rate computed from CFD, which is obtained by dividing the average mass flow rate at the inlet or discharge by the average density.

The isentropic efficiency is computed using:

$$\eta_{is} = \frac{P_{is}}{P_{shaft}}, \tag{13}$$

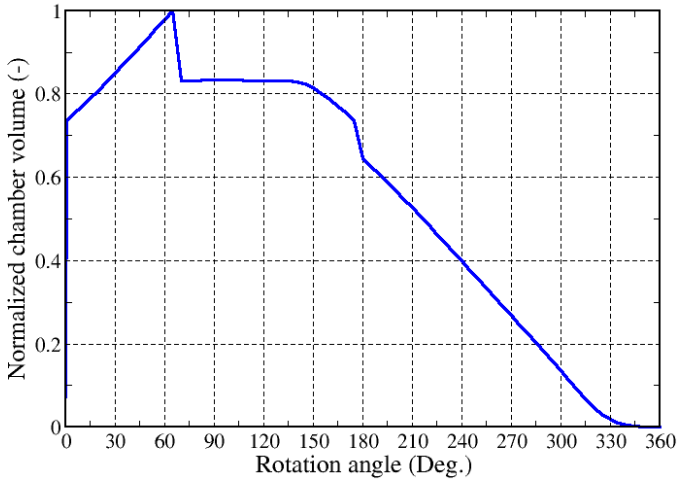

Figure 4. : Plot of the chamber volume of a claw pump

In case there is under or over compression, which is usually the case, the isentropic power P^*_{is} in equations 8 or 9 is used. In the initial or concept phase of the design, the shaft power may not be known. In this case CFD can be used to determine the pump power, which is less than the shaft power due to the extra power needed to run the gears and bearings and fan, in case there is a fan connection for cooling. Estimating the fan power and the losses due to the bearings and gears, it will be possible to predict the shaft power and hence the isentropic efficiency.

2.1. Volume curve generation

To be able to generate the chamber model presented in the previous section the volume curve as a function of the rotational angle is needed. One way of doing this is to use a CAD tool, in this

case, Inventor Professional. The volume curve is generated for the claw pump from 0° to 360° using an angular increment of 5° as shown in Figure 4. With this, it is possible to determine the volumes at the various stages of the pump shown in Figure 1(b) and hence the model parameters presented in section 2. The volume curve begins at suction followed by transport, followed by the compression and the discharge. In one cycle, the process of the carried-over volume occur twice as expected.

3. CFD case setup

The simulated geometry of the claw pump is generated using Inventor Professional. By using this CAD tool and ANSYS Design Modeler [1] the fluid volume was extracted from the CAD model and exported as an stl file to CONVERGE Studio [7]. As a pre-processor, CONVERGE Studio was used. It is important to note that the cartesian mesh generation in this tool is automated. Therefore, only the boundaries and the numerical parameters have to be specified. The simulations of the unsteady, turbulent flow were carried out using the Reynolds Average Navier Stokes (RANS) and the Pressure Implicit with Splitting Operators (PISO) solver implemented in the CONVERGE solver. As an equation of state the ideal gas law was chosen because it depicts the behavior of air very well for moderate pressures. The mesh size was influenced by the base grid, adaptive mesh refining based on temperature and velocity gradients and fixed embedding for the geometry were used. For the base grid, 8 mm was chosen. The simulations are done in parallel using MPI and the CONVERGE solver using a Linux Solver with 8 cores and 256 GB RAM. For turbulence modeling, the $k-\varepsilon$ model is used with the law of the wall using the standard wall function [6]. Post-processing is done using EnSight.

Table 1. Flow regimes

Continuous flow	0	$<$	Kn	$<$	0.01
Sliding flow	0.01	$<$	Kn	$<$	0.1
Knudsen flow	0.1	$<$	Kn	$<$	10
Free molecular flow	10	$<$	Kn		

In doing the case setup it is important to consider the type of flow and this is described by its Knudsen number Kn that is defined by $Kn = \frac{\lambda}{l_{char}}$, which is the ratio of the mean free path length λ to the characteristic length l_{char} [5]. The different type of flows are shown in Table 1 [4]. In a sliding flow the collisions between gas particles still occur often but the no-slip condition of continuum mechanics is no longer valid. Inside a Knudsen (transitional) flow collisions between two molecules are about as often as collisions between molecules and walls. The Navier-Stokes equation can only be applied to the continuous and sliding flow [5]. It is important to point out that the solver took longer at lower suction pressures due to the larger velocity gradients in the flow at these pressures.

For the cases reported here the solid rotors and pump housing are not included in the simulation. The gap modelled is therefore the cold gap. To model the hot gap, sealing or gap models are used in CONVERGE Studio to decrease the axial gaps on the drive and the non-drive sides and the radial gaps between the pump housing and the rotors and that between the rotors. To account for the thermal expansion of the rotors and their effect on the gaps inside the machine a combination of Conjugate Heat Transfer (CHT) and Fluid-Structure-Interaction (FSI) simulations are needed.

Figure 5 shows a sketch of the pump setup used in the CFD and in the measurement. It shows the suction side denoted by using the subscript S and the discharge side shown by using the subscript D. The suction valve and the silencer are not included in the CFD simulations.

3.1. Measurement setup

For measurements, the setup shown in Figure 5 is used. It shows the pump being measured and temperature and pressure sensors are used to measure the suction pressure and temperature and the discharge pressure and temperature. The shaft torque is also measured using a torque meter. The volume flow rate or pumping speed is also measured for various suction pressures upto 75 mbar abs. The point of ultimate vacuum (almost zero mass flow rate) was not reached because of the high thermal loads on the rotors and sealing that can result in rotor-to-housing or rotor-to-rotor contact. The measurement was carried out at a speed of 60 Hz or 3600 rpm, but it is possible to run the machine at 50 Hz or 3000 rpm or at other speeds using a variable frequency drive (VFD).

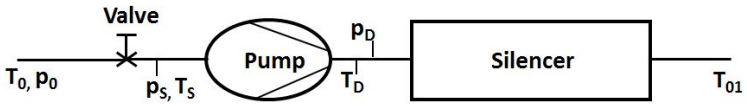

Figure 5. : Schematic of the setup used in the CFD simulations and measurements

4. Results and discussions

To be able to use CFD and the 0-D thermodynamic model in the design process benchmarking is required. To do this, a baseline case is selected and simulations are run for this case and validated with measurement data. Sealing, which helps with predicting the hot gaps inside the machine are used in CONVERGE Studio to ensure that the right losses are being predicted by the solver. When the machine is designed, the gaps included are the cold gaps but in reality the machine heats up when it runs and the thermal expansion of the rotors and the housing will change the radial and axial gaps inside the machine.

In the following, the baseline case results and validation with measurement data are presented. Grid dependency studies are performed to ensure that the results obtained are physical. This is followed by results to predict the entire performance map of the baseline machine simulated. In each case, validation is done with measurement data. Comparison to the 0-D model, which is the ideal case, is also done. Results for the pumping speed, pump power and the volumetric efficiency and isentropic efficiency are presented.

Table 2. Comparison of measurement and simulated data.

Parameter	CFD	Measurement	% error
Norm. pump power (-)	0.91	1.0	9
Norm. mass flow rate(-)	1.0	0.91	10
Norm. female rotor avg. torque (-)	1.0	-	-
Norm. male rotor avg. torque (Nm)	0.56	-	-

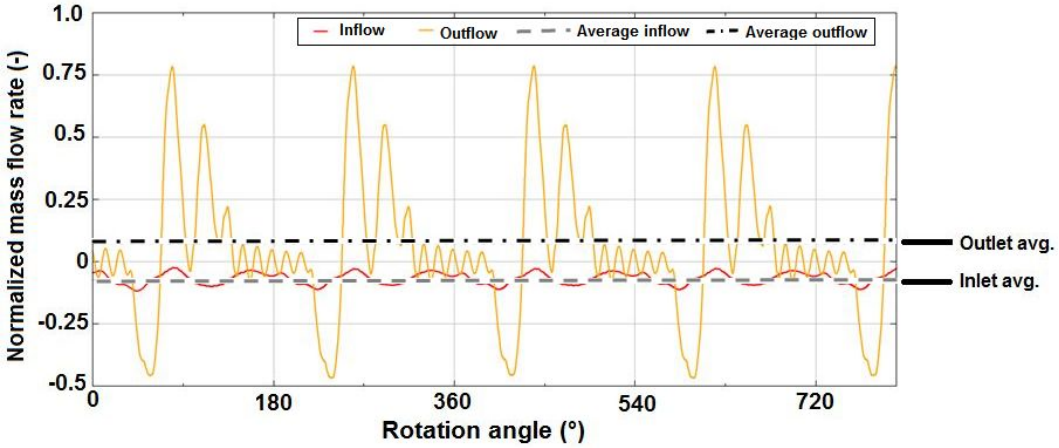

(a) Mas flow rates at inlet and discharge

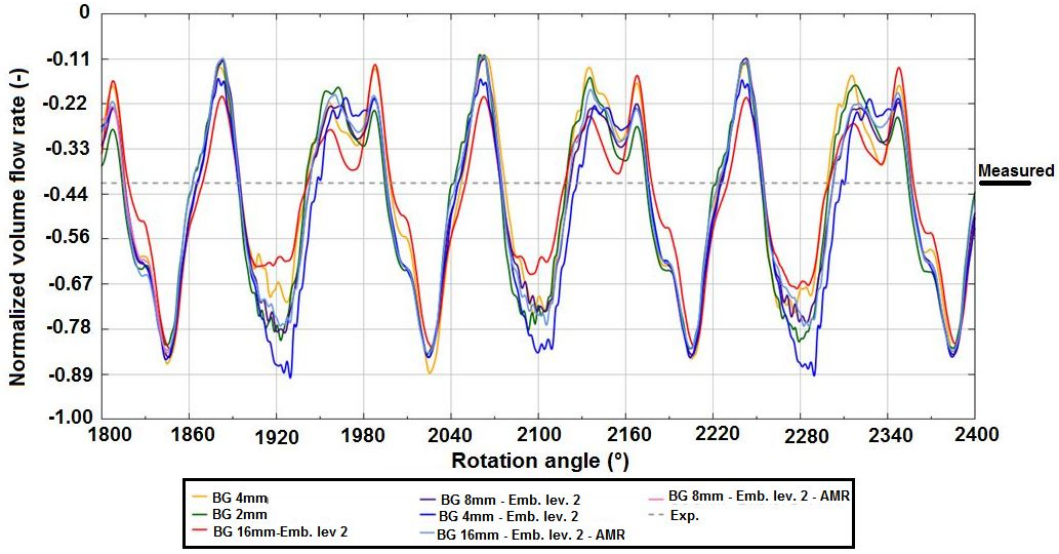

(b) Volumes flow rates at inlet

Figure 6. Plots of the mass flow rate and the volume flow rates at the inlet and discharge computed from CFD

4.1. Grid dependency studies

For grid independent studies, an operating point with a suction pressure of 150 mbar abs. is selected. The mass flow rates and hence the volume flow rates and the male and female rotors power are monitored and compared to measurement data as shown in Figure 6 and Table 2. In Figure 6, the normalization is done using the maximum mass flow rate and the maximum volume flow rate plotted from CFD. In Table 2, the pump power is normalized using the measured pump power. For the mass flow rate in Table 2, the average mass flow is determined from CFD and this value is used in the normalization. The torques are normalized using the average female rotor torque. Even though we are operating in vacuum, the principle of mass conservation at the boundaries of our pump applies. The mass entering must equal the mass leaving the pump. Due to the small gaps inside such machines and the high velocity gradients, especially at low suction pressures, the flow is simulated as compressible. The base grid and the level of embedding and AMR (Adaptive Mesh Refinement), based on the temperature and the velocity gradients were

changed until a mesh independent solution was obtained [7]. The goal was to obtain a mesh independent solution while at the same time limiting the computational cost. Because the solver is semi-implicit, it is possible to change the Courant-Friedrichs-Lewy (CFL) number depending on the gradients in the flow. The mesh parameters are specified and the meshing itself is done automatically, which allows for more flexibility. For boundary conditions, pressure inlet and pressure outlet are used. The mass flow is computed by the solver as a result. Constant wall temperatures are specified and heat transfer within the fluid and between the fluid and the wall is considered but the solid rotors and pump housing are not included in the simulation.

In Table 2, it is important to note that the female rotor torque is greater than the male torque as expected because it transport a larger volume of fluid than the male. The difference between the computed pump power and the measured is due to the fact in the measurement the torque is that of the input shaft which runs the gears and overcomes other losses in the bearings, sealing, etc. which are not accounted for in the CFD simulations.

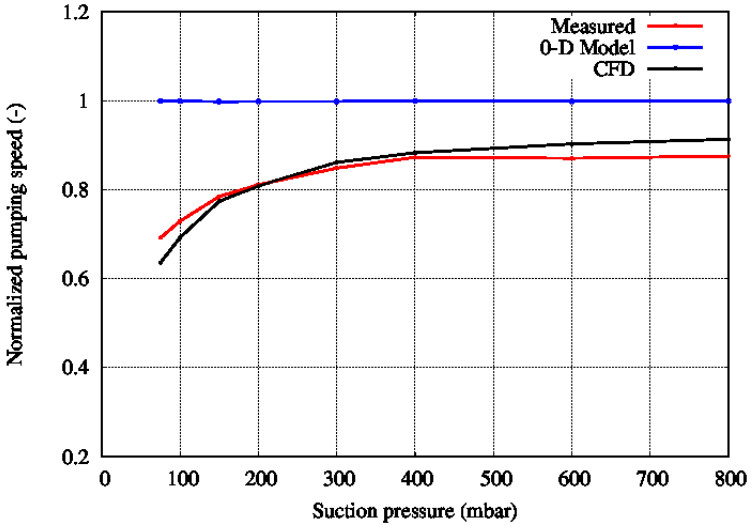

Figure 7. : Measured and predicted claw pump normalized pumping speed verses suction pressure

4.2. Performance prediction and optimization

Performance prediction is crucial in the design of vacuum pumps. The right motor and pumping speed must be predicted as well as critical parameters like bearings temperature, air discharge temperature, cooling needed, etc., before the prototype is developed and tested. In the following, the performance predicted for a typical claw pump is presented. Using the 0-D model presented in section 2 it is possible to do such prediction. CFD can also be used with a greater degree of accuracy because it includes the losses due to gaps inside the machine as well as the 3D and dynamic effects due to the rotation of the rotors and the interaction between the various chambers. In both cases presented, validation is done with measurement data. In Figure 7, the normalized pumping speed, which is normalized using the maximum computed pumping speed from the 0-D model is presented. The measured curve is closer to the predicted CFD curve than to the 0-D model since the latter does not account for the gap flow or losses inside the machine. The CFD prediction is better in terms of the trend at higher suction pressure than at lower suction pressure because of the high gradients associated with the flow at lower suction pressure.

The plot of the pump power normalized using the maximum shaft power measured is shown in Figure 8. The CFD model does not account for the power consumed by the gears and bearings and other losses accruing in the sealing but the trend is similar between the CFD and measurements results, unlike the pumping speed. If the power versus suction pressure is plotted for the 0-D model, it would show a linear increase from high suction pressure to low suction pressure since the over-compression at the high suction pressure that leads to high power consumption is not accounted for in the 0-D model.

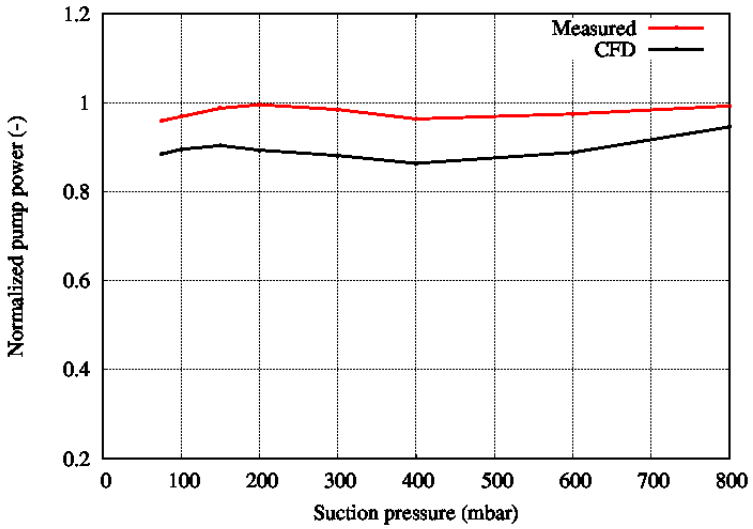

Figure 8. : Performance curve of the power of a claw pump: Measured versus predicted

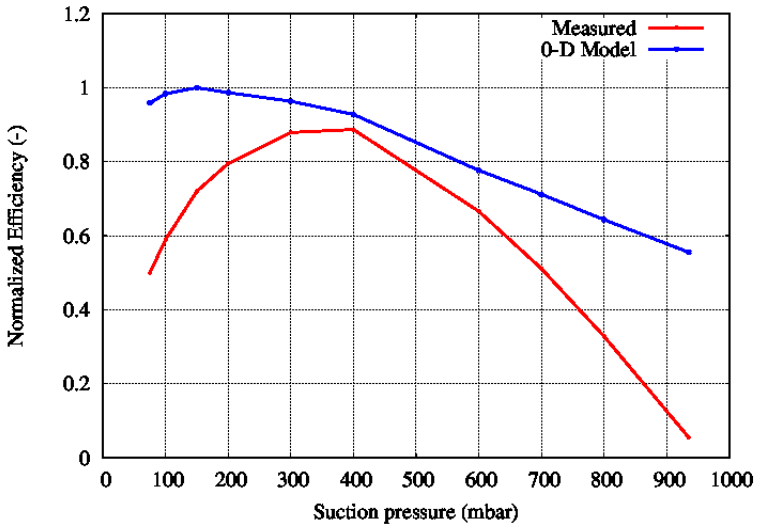

Figure 9. : Performance curve of the isentropic efficiency of a claw pump: Measured versus predicted

In Figure 9, the plot of the pump isentropic efficiency is shown. It shows similar trends: lower on the high pressure side due to over compression and it decreases on the low pressure side due

to under-compression and increase in leakages due to high velocity gradients in the flow. It is maximum at the design point where there is no under or over compression. For the measured isentropic efficiency equation 13 is used. The efficiency of the 0-D model is computed by using P^*_{is} in equation 13 instead of P_{is} and P_{shaft} is obtained by using the measured torque and the rotational speed.

One of the goals of this work was to carry out an engineering optimization of the pump investigated. As an example, the discharge tube is optimized using 3D CAD in combination with 3D CFD. The pump power relative to the baseline (benchmark) case is computed and presented in Figure 10. In this case, the optimization parameter that was selected for minimization was the pump power since pressure drop will not be appropriate because of the pressure inlet and outlet boundary conditions used. Clearly, design 3b is the best design since it offers the highest power saving achievable of the cases considered. The worst case was design 3 since it has the highest power consumption relative to the baseline case.

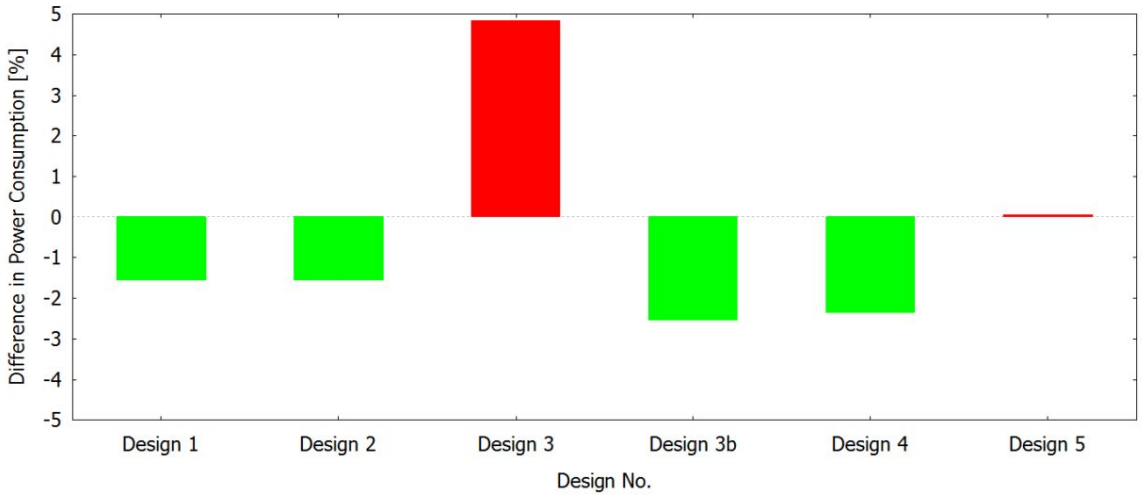

Figure 10. : Optimization of the discharge tube of claw pump

5. Conclusions

This paper presents the successful simulation of the flow inside a claw vacuum pump using 3D CFD. Simple 0-D thermodynamic model as well as 3D CFD results and validation with measurement data are presented. Using the 0-D thermodynamic model the compression ratio (π), the built-in volume ratio (θ), the volume compression ratio (v_i) and the intermediate pressures (p_z, p_i) as well as the ideal volume flow rate were determined during the concept phase. 3D CFD was used to determine more accurately the performance parameters like the pumping speed and the pump power. An existing claw pump with measurement data is used as a benchmark for validating the CFD process after which engineering optimization of the pump is done. The discharge tube is optimized with the goal of reducing the pump power as presented. The following are planned for future work:

- Using CFD with heat transfer to be able to predict the temperature of the rotors and housing of the pump. The heat flux and pressure distribution on the rotors can be used for computing the deflection or deformation of the rotors. This information is useful in sizing the gaps inside the pump. With this it will be possible to determine the hot gaps inside the pump.

- Flow optimization to reduce leakages and extend the vacuum range of the pump
- Extension of the chamber model to include flow losses or leakages and heat transfer

Nomenclature

θ	Internal volume ratio	[-]
κ	Isentropic exponent	[-]
π	Internal compression ratio	[-]
ρ	Density	[kg/m^3]
$\dot{m}$	Mass flow rate	[kg/s]
T	Torque	[Nm]
N	Rotational speed	[1/s or Hz]
p	Pressure	[Pa]
p_D	Discharge pressure	[Pa]
p_i	Pressure before opening of the outlet	[Pa]
p_S	Suction pressure	[Pa]
p_z	Pressure when the carried-over volume is separated	[Pa]
P_{is}	Isentropic or ideal power	[W]
P^*_{is}	Power with under or over-compression	[W]
V	Volume	[m^3]
V_i	Volume before opening the outlet	[m^3]
V_R	Carried-over volume	[m^3]
V_{RS}	Expanded carried-over volume	[m^3]
V_{S1}	Volume of chamber 1	[m^3]
V_{S2}	Volume of chamber 2	[m^3]
$\dot{V}$	Pumping speed or volume flow rate	[m^3/s]
V_{th}	Theoretical volume flow rate or pumping speed	[m^3/s]
V_S	Ideal volume flow rate or pumping speed	[m^3/s]
η_V	Volumetric efficiency	[%]
η_{is}	Isentropic efficiency	[%]
z	Number of teeth	[-]
λ	Free mean path length	[m]
l_{char}	Characteristic length	[m]

Acknowledgment
The authors would like to thank Dr. David Rowinski of Convergent Science for his invaluable support. His valuable contribution is acknowledged.

References

[1] ANSYS 2018 *DesignModeler User Guide*, Release 18.0 (ANSYS, Inc.)
[2] Faragallah W H 2008 *Vakuum Pumpen (Gastransfervakuumpumpen)*, (Sulzbach: Verlag und Bildarchiv w.H. Faragallah)
[3] Fister W 2013 *Fluidenergiemaschinen: Physikalische Voraussetzungen, Kenngrößen, Elementartstufen der Strömungs-und Verdrängermaschinen*, (Berlin: Springer-Verlag, Band 1)
[4] Frohn A 1979 *Einführung in die kinetische Gastheorie: Studienbuch für Studierende der Ingenieurwissenschaften, der Physik und der physikalischen Chemie*, (Akademische Verlagsgesellschaft)
[5] Müller R 2013 *Spaltströmung mit Wärmeübertragung in Vakuumpumpen*, PhD thesis. Universität Kaiserslautern
[6] Pope S B 2000 *Turbulence Flows*, (Cambridge University Press, ed 1)
[7] Richards J K, Senecal P K and Pomraning E 2017 *Converge 2.4 Manual*, Madison, WI (Convergent Science, Inc.)